International Journal of Thermophysics, Vol. 25, No. 4, July 2004 (© 2004)

Thermophysical Properties of 1,1,1,3,3-Pentafluorobutane (R365mfc)[1]

A. P. Fröba[2], K. Krzeminski[2], and A. Leipertz[2,3]

This paper presents an experimental study on various thermophysical properties of a new fluoroalkane, 1,1,1,3,3-pentafluorobutane (R365mfc). The thermal conductivity of R365mfc was measured in the liquid phase near saturation conditions at temperatures between 263 and 333 K using a parallel plate instrument with an uncertainty of less than ±5%. For the measurement of the saturated liquid density between 273 and 353 K, a vibrating tube instrument was used. The uncertainty of the density measurements is less than ±0.1%. In addition, experimental data have been obtained for R365mfc under saturation conditions over a wide temperature range from about 253 to 460 K using light scattering techniques. Light scattering from the bulk fluid has been applied for measuring both the thermal diffusivity and the sound speed in the liquid and vapor phases. Light scattering by surface waves on a horizontal liquid–vapor interface has been used for the simultaneous determination of the surface tension and kinematic viscosity of the liquid phase. With the light scattering techniques, uncertainties of less than ±1.0, ±0.5, ±1.0, and ±1.2% have been achieved for the thermal diffusivity, the sound speed, the kinematic viscosity, and the surface tension, respectively.

KEY WORDS: density; kinematic viscosity; R365mfc; sound speed; surface tension; thermal conductivity; thermal diffusivity.

1. INTRODUCTION

The 1,1,1,3,3-pentafluorobutane (R365mfc) is a new hydrofluorocarbon which is mainly used for the production of rigid polyurethane foams for

[1]Paper presented at the Fifteenth Symposium on Thermophysical Properties, June 22–27, 2003, Boulder, Colorado, U.S.A.

[2]Lehrstuhl für Technische Thermodynamik (LTT), Friedrich-Alexander-Universität Erlangen-Nürnberg, Am Weichselgarten 8, D-91058 Erlangen, Germany.

[3]To whom correspondence should be addressed. E-mail: sek@ltt.uni-erlangen.de

0195-928X/04/0700-0987/0 © 2004 Plenum Publishing Corporation

insulation purposes where a liquid foaming agent with a low thermal conductivity and a high vapor pressure at low temperatures is needed. On account of the thermodynamic properties and of safety requirements, R365mfc is employed as a main component in binary blends with 7 or 13 mass% 1,1,1,2,3,3,3-Heptafluoropropane (R227ea) in the production of liquid foaming agents [1]. Besides the fact that no impact on the ozone layer can be found, further environmental benefits can be addressed using R365mfc in the production of polyurethane foams. Thus, life cycle assessments have demonstrated that such product systems due to their high insulation capacity, which reduces energy consumption and consequently the contribution to global warming, can be more eco-efficient than alternative solutions based, e.g., on water as a blowing agent [2]. At present, another field of application, which is under active consideration, is the use of R365mfc as a possible working fluid in high-temperature heat-pump systems at condensation temperatures of about 100 °C. Here, the use of R365mfc as a main component in binary blends with R227ea can save energy to a great extent by utilization of the temperature glide of the mixture [3].

As it is not possible to experimentally determine all the required properties of hydrofluorocarbon mixtures in a large variety of thermodynamic states, models based on the data of the pure substances are employed, see, e.g., Refs. 4–8. Yet, this approach fails for the aforementioned blends with R365mfc as a main component. A literature survey reveals that only a very limited number of data is available for R365mfc. This situation holds both for equilibrium data and is even more pronounced for transport properties. Thus, only one experimental study can be found in the literature which reports values for the vapor pressure, vapor-phase thermal conductivity, and liquid density of R365mfc [9]; and data for the upper temperature region are only obtained from lower temperature values by extrapolation and are completely lacking for the critical region. It is the major aim of this work to contribute to the verification and improvement of the data situation for R365mfc. In the present paper, first, the methodological principles and experimental conditions for the measurement techniques used for the determination of density, thermal conductivity, thermal diffusivity, sound speed, viscosity, and surface tension are briefly reviewed. Then, the experimental results for R365mfc are presented and compared with the few reference data available.

2. EXPERIMENTAL METHODS

For all experiments the same R365mfc sample has been used. According to the specification of the manufacturer (Solvay Fluor & Derivate

GmbH, Hannover), the sample had a purity of $\geqslant$99.5% and was used without further purification.

2.1. Vibrating Tube Method for Density

For the liquid density measurements the vibrating tube method was used, where a hollow U-shaped tube is forced into harmonic oscillation. The period of oscillation is dependent on the density of the sample in the tube. Therefore, by measuring the period of oscillation, the density is calculated. For the density meter (DMA 5000, Anton Paar) used here a reference oscillator is built into the measuring cell which eliminates long-term drift and only one adjustment at 20 °C is sufficient to reach a high accuracy for the whole measuring temperature range. The DMA 5000 allows a full-range viscosity correction, whereby all viscosity related errors inherent to all known types of oscillating U-tube density meters are automatically eliminated. The temperature of the U-tube is controlled within $\pm$1 mK with the help of Peltier elements and measured by a high-precision platinum resistance probe with an uncertainty of $\pm$10 mK. For the calibration of the density meter, standard water and air were used. Before measuring the saturated liquid density of R365mfc, the U-tube was evacuated. Then the sample was filled from the liquid phase into the U-tube of the density meter.

2.2. Parallel-Plate Instrument for Thermal Conductivity

For measuring the thermal conductivity of R365mfc in its liquid phase near saturation conditions, a parallel-plate instrument was used which is designed to fulfill as close as possible the ideal one-dimensional form of the Fourier law of heat conduction. For this purpose a fluid layer located in a narrow gap between two horizontal plates is subjected to a stationary temperature gradient and the dependence of the heat flow on this gradient is measured. The quantities which are measured during the experiment are the dissipated power in the upper plate to maintain a stationary temperature gradient and the temperature difference between the upper and lower plates. Furthermore, for evaluation of the thermal conductivity the thickness of the fluid layer and the effective area of the upper plate have to be known.

In our apparatus the two parallel plates are made of copper. All other parts of the instrument are made of stainless steel. The surfaces of the lower plate (diameter, 146 mm) and upper plate (diameter, 86 mm) which are in contact with the sample fluid are polished flat and they are covered with a thin chrome layer. Thus, the contribution of radiation on the

total heat flow is small compared to that caused by heat conduction. In this work, however, radiation corrections have not been applied. The error introduced by neglecting the radiation contribution could be estimated to be within ±1% for the thermal conductivity of R365mfc. To ensure that the dissipated power in the upper plate results only in a heat flow through the fluid layer to the lower plate, the ambient environment of the upper plate is controlled by a special guard system. This consists of a guard ring in which the upper plate is immersed and a guard plate located above the upper plate. All parts of the guard system are maintained at the same temperature as the upper plate. While the temperature control for the guard ring and guard plate as well as for the upper plate is realized by resistance heating, the lower plate of the apparatus can be heated or cooled with help of Peltier elements. For temperatures below room temperature, the complete parallel-plate instrument is surrounded by an insulated housing which can be cooled by a lab thermostat about 10 K below the desired temperature inside the liquid layer. The temperatures of all control circuits of our parallel-plate instrument are measured using calibrated 100 Ω platinum resistance probes with an absolute uncertainty of ±0.1 K. The relative uncertainty of the resistance probes among each other was less than ±0.01 K.

In the present study the thermal conductivity cell was filled with the liquid sample at ambient conditions. For temperatures between 263 and 303 K thermal conductivity measurements were carried out at atmospheric pressure. When exceeding the normal boiling point of R365mfc ($T_b = 313.35$ K [10]), measurements were performed in the compressed liquid phase at a maximum pressure of about 3 bar and are expected to be slightly higher than measurements at saturation. For each temperature point three independent measurement series have been performed where the gap between the two plates was adjusted to 0.5, 1.0, and 1.5 mm by three micrometer screws within an uncertainty of ±0.01 mm. For all measurements the temperature difference ΔT between the lower and upper plates was adjusted to 3 K. Thus, the applied temperature gradient was only varied by changing the sample thickness d between the two plates. Assuming that residual parasitic heat flows $\dot{Q}_c$ are independent of the gap between both plates, the determination of the thermal conductivity λ has been performed according to

$$\dot{Q}_{exp} = -\lambda A \frac{\Delta T}{d} + \dot{Q}_c \tag{1}$$

by plotting the measured dissipated power $\dot{Q}_{exp}$ in the upper plate against the applied temperature gradient $\Delta T/d$. In Eq. (1) A represents the effective area of the upper plate. Finally, values for the thermal conductivity

have been obtained by fitting the dependence of the measured dissipated power on the temperature gradient by a linear equation. Before starting the thermal conductivity measurements for R365mfc, our parallel-plate instrument was checked by measuring the thermal conductivity of liquid water and ethanol over a temperature range from 303 to 363 K. The values obtained are in agreement with the standard reference data for water [11] and tabulated literature data for ethanol [12], for which the maximum deviations are less than 3 and 2%, respectively. More information on this apparatus is given in Ref. 13.

2.3. Thermal Diffusivity and Sound Speed by Light Scattering from Bulk Fluids

The principle of dynamic light scattering (DLS) for the determination of thermal diffusivity and sound speed is given in detail elsewhere, see e.g., Refs. 14–17. Here, only the essential features are repeated. DLS probes the spectrum of light scattered by a fluid in macroscopic thermodynamic equilibrium. For a pure fluid the underlying scattering process is governed by microscopic fluctuations of temperature (or entropy) and of pressure. Information about these processes can be derived through a temporal analysis of the scattered light intensity by using photon correlation spectroscopy (PCS). With the exception of a region in the vicinity of the critical point, this is commonly done by applying a heterodyne technique, where a reference beam is added to the scattered light. In this case, the intensity correlation function is of the form,

$$G^{(2)}(\tau) = A + B\exp(-\tau/\tau_C) \tag{2}$$

with experimental constants A and B, where B is essentially determined by the ratio of scattered light and reference light and the coherence properties of the optical system. From the measured correlation time, τ_C, which is equivalent to the mean life time of the temperature fluctuations observed, the thermal diffusivity a can be calculated by

$$a = \frac{1}{\tau_C q^2}, \tag{3}$$

where the modulus of the scattering vector q is determined along with the laser wavelength in vacuo by the scattering geometry of the experiment, see, e.g., Ref. 17.

For the measurement of the sound speed u_S the periodic pressure fluctuations are probed which can be understood as sound waves. In practice, the frequency ω_S of the sound waves is determined by adding a reference beam,

which is shifted relative to the frequency ω_0 of the laser light by $\Delta\omega_M$ applying an acousto-optical modulator. The frequency shift $\Delta\omega_M$ is of the same order of magnitude as the frequency of the sound waves ($\Delta\omega_M \approx \omega_S$). In this case, the correlation function takes the form,

$$G^{(2)}(\tau) = A + B\exp(-\tau/\tau_C)\cos(\Delta\omega\tau), \tag{4}$$

and the sound speed u_S can be found from a knowledge of the adjusted modulator frequency $\Delta\omega_M$ and the residual detuning $\Delta\omega$ according to

$$u_S = \frac{\omega_S}{q} = \frac{\Delta\omega_M \pm \Delta\omega}{q}. \tag{5}$$

The experimental setup used here for the determination of thermal diffusivity and sound speed is the same as was employed in our former investigations for toluene and is described in more detail in Refs. 18 and 19. The R365mfc sample was kept at saturation conditions inside a cylindrical thermostated pressure vessel (inner diameter, 18 mm; volume $\approx 10\,\text{cm}^3$) equipped with two quartz windows (Herasil I; diameter, 30 mm; thickness, 30 mm). The actual temperature in the sample cell which was placed in an insulating housing was regulated through resistance heating with a longterm stability better than 10 mK. The vessel temperature was measured with a calibrated 25 Ω platinum resistance probe integrated into the main body of the measuring cell with a resolution of 0.1 mK using an ac bridge (MKT 25, Anton Paar). The uncertainty of the temperature measurement was better than ±5 mK. For each temperature point, typically six measurements at different values for the modulus of the scattering vector q have been performed.

2.4. Viscosity and Surface Tension from Surface Light Scattering

In the following, the underlying theory of surface light scattering (SLS) is briefly reviewed. For a more detailed and comprehensive description the reader is referred to the specialized literature [20, 21]. SLS is a technique which is closely related to DLS in its classical form. The difference is that this technique probes, as the name indicates, fluctuations on the surface of a liquid or, in a more general formulation, at phase boundaries. Liquid–vapor interfaces in macroscopic thermal equilibrium exhibit surface waves which are caused by thermal movement of molecules and which are quantized in so-called "ripplons." For small viscosities, as is relevant in the experiments described here, the amplitude of surface waves decays in the form of a damped oscillation. SLS analyzes the light scattered by these surface waves.

Here again the experiments are based on a heterodyne detection scheme and signal analysis by PCS. The correlation function of light scattered by surface fluctuations may be described by

$$G^{(2)}(\tau) = A + B\exp(-\tau/\tau_C)\cos(\omega_R\tau), \tag{6}$$

where the correlation time τ_C and the frequency ω_R are identical with the decay time and the frequency of the surface oscillations observed, respectively. In first-order approximation the ratio of the sum of the dynamic viscosities of the liquid phase η' and vapor phase η'' to the sum of the densities of the liquid phase ρ' and vapor phase ρ'' may be obtained from the decay time τ_C by

$$\frac{\eta' + \eta''}{\rho' + \rho''} \approx \frac{1}{2\tau_C q^2}. \tag{7}$$

Furthermore, the correlation function Eq. (6) can simultaneously be evaluated for the ratio of the surface tension σ to the sum of the densities of the vapor and liquid phases,

$$\frac{\sigma}{\rho' + \rho''} \approx \frac{\omega_R^2}{q^3}, \tag{8}$$

which in first-order approximation directly follows from the beat frequency ω_R and the wave vector q.

For a reliable determination of viscosity and surface tension a more detailed and rigorous consideration of the SLS method than given by Eqs. (6)–(8) has to be applied. In the present work, however, data for the liquid kinematic viscosity and surface tension were obtained by an exact numerical solution of the dispersion equation for surface waves at a liquid–vapor interface, see, e.g., Refs. 21 and 22, where the measured frequency ω_R, the damping $\Gamma(= 1/\tau_C)$, and the modulus of the wave vector q are used as input values.

The R365mfc sample was filled from the liquid phase into an evacuated cylindrical pressure vessel (inner diameter, 70 mm; volume, 150 cm^3) equipped with two quartz windows (Herasil I; diameter, 30 mm; thickness, 30 mm). The temperature regulation of the cell surrounded by an insulating housing was realized with electrical heating. For temperatures below room temperature, the insulating housing was cooled to about 10 K below the desired temperature in the sample cell using a lab thermostat. The temperature of the cell was measured with two calibrated 100 Ω platinum resistance probes, integrated into the main body of the vessel, with a resolution of 0.25 mK using an ac bridge (MKT 100, Anton Paar). The uncertainty of the absolute temperature measurement was better

Table I. Experimental Values of the Liquid Density ρ' of R365mfc Under Saturation Conditions

T (K)	ρ' (kg·m^{-3})	T (K)	ρ' (kg·m^{-3})
273.15	1308.2	323.15	1201.4
278.15	1298.0	328.15	1189.8
283.15	1287.6	333.15	1178.1
288.14	1277.3	338.15	1166.2
293.15	1266.7	343.15	1154.0
298.15	1256.5	348.15	1141.7
303.15	1245.7	353.15	1129.2
308.15	1234.9	358.15	1116.2
313.15	1223.8	363.15	1102.8
318.15	1212.7		

than ±15 mK. The temperature stability during an experimental run was better than ±1 mK. For each temperature, at least six measurements at different values for the modulus of the scattering vector were performed. For a detailed description of our SLS apparatus, the reader is referred to Refs. 21 and 23.

3. RESULTS AND DISCUSSION

3.1. Density

The experimental results for the density of the liquid phase of R365-mfc under saturation conditions are summarized in Table I. The listed data are average values of three independent measurement series with new samples within the U-tube of the density meter. These measurements agreed within ±0.03%. The total uncertainty of the density measurement is estimated to be less than ±0.1%. Within experimental uncertainty, the density data have been correlated with a simple polynomial equation,

$$\rho' = \sum_{i=0}^{3} \rho'_i (T/\mathrm{K})^i, \tag{9}$$

where the coefficients determined by least squares are, in units of kg·m^{-3}: $\rho'_0 = 2135.79$, $\rho'_1 = -5.34312$, $\rho'_2 = 0.013283$, and $\rho'_3 = -1.7628 \times 10^{-5}$. The root-mean-square deviation between the experimental data and Eq. (9) is 0.0072%.

In Fig. 1 the liquid density of R365mfc under saturation conditions has been plotted in the upper part in comparison with literature data. In

the lower part of Fig. 1 the deviations between the correlation, Eq. (9), developed from our experimental results and literature data are shown. Included in Fig. 1 are experimental data by Solvay [10] and Marrucho et al. [9]. The latter have determined the density of R365mfc using also the vibrating tube method, where an uncertainty of less than ±0.2% is stated. In addition to the measurement values, the correlation from Ref. 9 is shown which is based on a modified Rackett equation. Also shown in Fig. 1 are tabulated values from a data sheet of the manufacturer which is available via the internet [24]. Finally, liquid densities of saturated R365mfc data calculated by REFPROP [25] have been included in Fig. 1. These data are based on a REFPROP fluid file which was exclusively developed for the manufacturer Solvay by the National Institute of Standards and Technology (NIST). While our data show good agreement with the experimental data of Marrucho et al. [9] for the complete temperature range within combined uncertainties, their proposed correlation in the form of a modified Rackett equation not only exhibits systematic deviations with respect to our density values but also fails to represent their own data well within the stated uncertainty. Excellent agreement between our data and those calculated by REFPROP [25] is found, where the maximum deviation is +0.075% at 273.15 K.

3.2. Thermal Conductivity

Values obtained for the thermal conductivity of R365mfc near saturation conditions for the liquid phase by our parallel-plate instrument are listed in Table II and are plotted in Fig. 2. Here, the given temperatures represent the average temperatures in the fluid layer between the upper and lower plates of our instrument. The thermal conductivity data have been correlated by a simple linear equation,

$$\lambda = \lambda_0 + \lambda_1 (T/\mathrm{K}) \tag{10}$$

with $\lambda_0 = 0.2364\,\mathrm{W{\cdot}m^{-1}{\cdot}K^{-1}}$ and $\lambda_1 = -0.494 \times 10^{-3}\,\mathrm{W{\cdot}m^{-1}{\cdot}K^{-1}}$. The maximum deviation between the experimental data and Eq. (10) is about 3.0%, which is within the estimated uncertainty of ±5.0%. Since there are no literature data available for the thermal conductivity of R365mfc in the liquid phase, data comparisons could not be performed here.

The same statement also holds for the following sections, where values for the thermal diffusivity, sound speed, kinematic viscosity, and surface tension observed by light scattering techniques represent to the best of our knowledge the first data sets published for R365mfc.

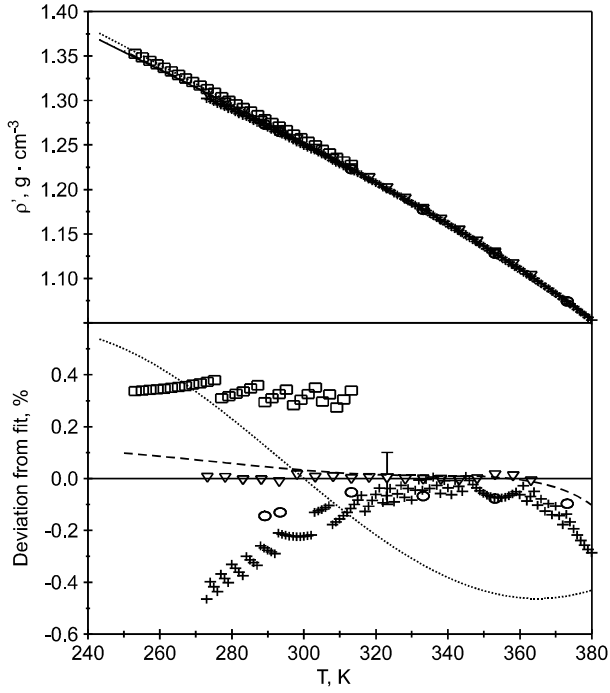

Fig. 1. Liquid density ρ' of R365mfc under saturation conditions in comparison with literature data. ▽—- this work; ○..... Marrucho et al. [9]; + SOLVAY [10]; □ SOLVAY [24]; – – REFPROP [25].

Table II. Experimental Values of the Thermal Conductivity λ of R365mfc in the Liquid Phase Near Saturation Conditions

T (K)	λ (mW·m^{-1}·K^{-1})
263.15	104.7
273.15	102.0
283.15	96.7
293.15	92.3
303.15	85.7
313.15	83.9
323.15	76.7
333.15	70.2

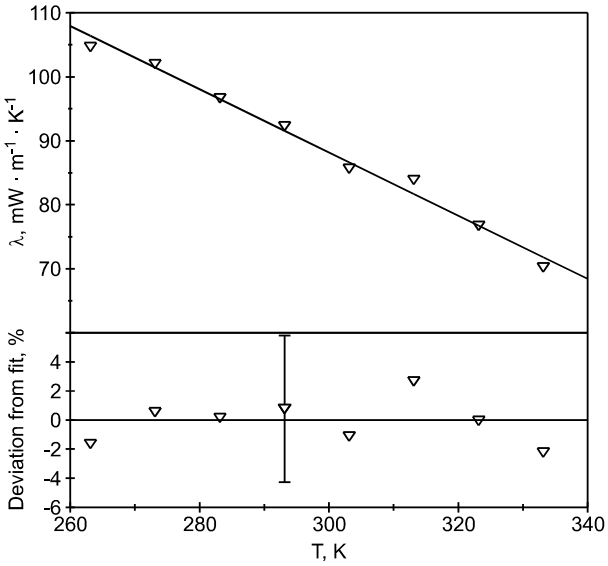

Fig. 2. Thermal conductivity λ of R365mfc in the liquid phase near saturation conditions.

3.3. Thermal Diffusivity and Sound Speed

The experimental data for the thermal diffusivity and sound speed obtained by light scattering from bulk fluids are plotted in Figs. 3 and 4, respectively, and are summarized in Table III. In the figures the lines are empirical correlations of our experimental data, and the open and closed symbols distinguish between the liquid and vapor phases, respectively. Each temperature point comprises six single measurements, the mean value of which is displayed. The standard deviation of the single measurements may be regarded as a measure for the uncertainty of DLS data [26]. Thus, the uncertainties of the measured data for R365mfc could be estimated to be less than ±1% for the thermal diffusivity and less than ±0.5% for the sound speed. For the highest temperatures studied in this work the measurement uncertainty for the thermal diffusivity and sound speed increases to about ±2 and ±1%, respectively. The reason for this behavior can be found by an increasing experimental complexity in the critical region.

The experimental data for the thermal diffusivity as well as for the sound speed for both vapor and liquid phases can well be represented by a sum of a polynomial and an additional term, which takes into account the curvature towards the critical point, resulting in an equation of the form,

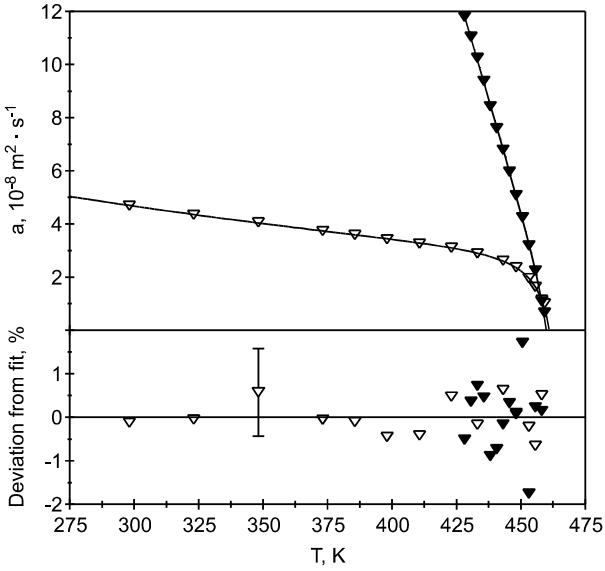

Fig. 3. Thermal diffusivity a of R365mfc under saturation conditions (▽, liquid phase; ▼, vapor phase).

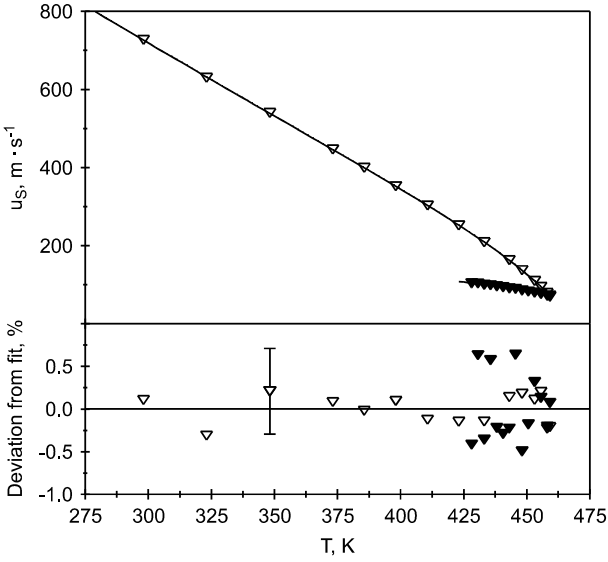

Fig. 4. Sound speed u_S of R365mfc under saturation conditions (▽, liquid phase; ▼, vapor phase).

Table III. Experimental Values of the Thermal Diffusivity a and Sound Speed u_S of R365mfc Under Saturation Conditions

Liquid phase			Vapor phase		
T (K)	a (10^{-8} m$^2 \cdot$ s^{-1})	u_S (m $\cdot$ s^{-1})	T (K)	a (10^{-8} m$^2 \cdot$ s^{-1})	u_S (m $\cdot$ s^{-1})
298.15	4.69	727.4	428.15	11.80	104.2
323.15	4.36	630.3	430.65	11.06	103.3
348.15	4.06	540.3	433.15	10.26	100.3
373.15	3.74	446.7	435.65	9.39	99.05
385.65	3.59	399.5	438.15	8.43	96.02
398.15	3.43	352.5	440.65	7.60	93.59
410.65	3.27	303.1	443.15	6.80	91.17
423.15	3.11	252.4	445.65	5.97	89.33
433.15	2.90	209.3	448.15	5.08	85.60
443.15	2.62	163.0	450.65	4.25	82.98
448.15	2.37	137.5	453.15	3.19	80.28
453.15	1.97	109.8	455.65	2.25	76.70
455.65	1.64	95.17	458.15	1.09	72.20
458.15	1.15	79.27	459.15		69.99
459.15		72.83			

$$y = \sum_{i=0}^{2} y_i (T/\mathrm{K})^i + \frac{y_3}{(T - T^*)/\mathrm{K}}, \tag{11}$$

where the coefficients y_i and the additional fit parameter T^* are given in Table IV. Here, also the root-mean-square deviations of our values from Eq. (11) and the ranges of validity of the correlations are stated. For both phases the root-mean-square deviations of our sound speed data from Eq. (11) is clearly less than 0.5%. Somewhat worse is the situation for the thermal diffusivity data, where a maximum root-mean-square deviation of 0.82% can be found for the saturated vapor phase.

3.4. Kinematic Viscosity and Surface Tension

The results for the liquid kinematic viscosity and surface tension of R365mfc under saturation conditions from surface light scattering are summarized in Figs. 5 and 6, respectively, and in Table V. The listed data are average values of at least six independent measurements with different angles of incidence. Also listed in Table V are values from the literature used for data evaluation as described below.

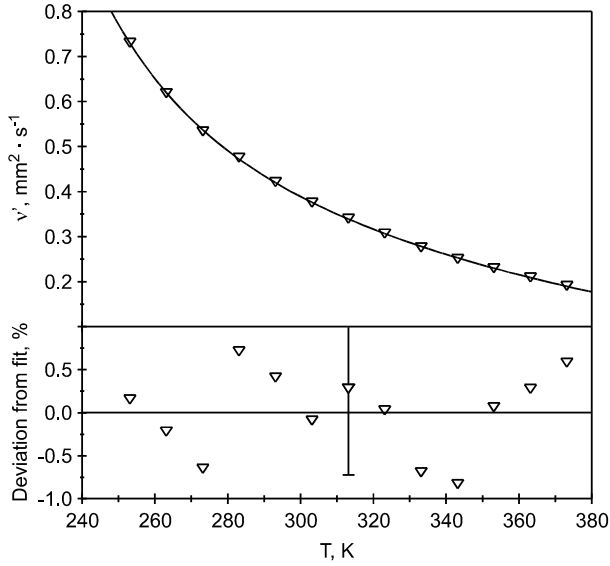

Fig. 5. Liquid kinematic viscosity ν' of R365mfc under saturation conditions.

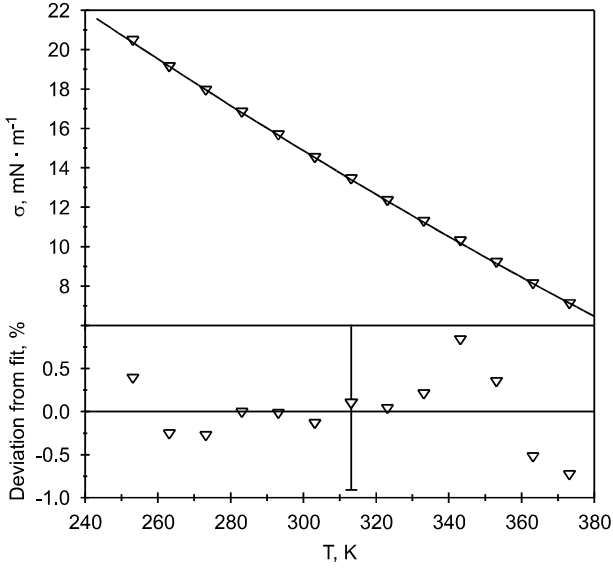

Fig. 6. Surface tension σ of R365mfc under saturation conditions.

Table IV. Coefficients of Eq. (11)

	Thermal Diffusivity $a\ y_i$ ($10^{-8}\,m^2\cdot s^{-1}$)		Sound Speed $u_S y_i$ ($m\cdot s^{-1}$)	
y_i	Liquid phase	Vapor phase	Liquid phase	Vapor phase
y_0	11.1672	174.5642	2032.37	−1081.24
y_1	−0.029097	−0.430555	−4.8988	6.2830
y_2	2.6065×10^{-5}	11.9152×10^{-5}	2.1102×10^{-3}	-8.2042×10^{-3}
y_3	18.487	7.489	6698.6	10.14
T^*(K)	466.70	464.25	502.38	461.64
Rms (%)	0.39	0.82	0.17	0.38
T-range (K)	298–458	428–458	298–459	428–459

Table V. Liquid Kinematic Viscosity ν' and Surface Tension σ of R365mfc Under Saturation Conditions[a]

T (K)	η'' ($\mu Pa\cdot s$) theoretically calculated	ρ' ($kg\cdot m^{-3}$) From Eq. (9)	ρ'' ($kg\cdot m^{-3}$) from Ref. 25	ν' ($mm^2\cdot s^{-1}$)	σ ($mN\cdot m^{-1}$)
253.15	8.75	1348.4	0.38	0.7311	20.44
263.15	9.11	1328.3	0.66	0.6190	19.11
273.15	9.49	1308.1	1.10	0.5340	17.92
283.15	9.88	1287.7	1.76	0.4760	16.80
293.15	10.3	1266.9	2.71	0.4218	15.65
303.15	10.7	1245.6	4.01	0.3761	14.50
313.15	11.1	1223.8	5.76	0.3403	13.42
323.15	11.5	1201.4	8.06	0.3072	12.32
333.15	11.9	1178.2	11.0	0.2767	11.26
343.15	12.3	1154.1	14.8	0.2511	10.27
353.15	12.8	1129.1	19.5	0.2303	9.18
363.15	13.2	1102.9	25.3	0.2097	8.09
373.15	13.6	1075.6	32.5	0.1910	7.09

[a] Directly measured values for frequency ω_R and damping Γ at a defined wave vector q of surface waves were combined with theoretically calculated values for η'', our own data for ρ', and data for ρ'' from Ref. 25 to derive ν' and σ by an exact numerical solution of the dispersion relation.

Data obtained from surface light scattering for the dynamics of surface waves, i.e., frequency ω_R and damping $\Gamma(=1/\tau_C)$ at a defined wave vector q, have been combined with reference data for the dynamic viscosity of the vapor phase η'' and density data for both phases ρ' and ρ'' to get information about the liquid kinematic viscosity ν' and surface

Table VI. Coefficients of Eq. (12)

ν'_0 ($mm^2 \cdot s^{-1}$)	29.266×10^6
ν'_1 (K)	–5337.27
ν'_2 (K^{-1})	–0.0241434
ν'_3 (K^2)	620890
rms (%)	0.47
T-range (K)	253–373

tension σ, see Section 2.4. While values for the liquid density are based on our own measurements, data for the vapor density have been adopted from Ref. 25. Data for the dynamic viscosity of the vapor phase have been calculated according to a method given in Refs. 27 and 28. Taking into account the uncertainties of the individual quantities entering into the calculation, the uncertainty of our liquid kinematic viscosity data is estimated to be better than ±1% for the complete temperature range investigated in this study. It should be noted that even approximate values for the dynamic viscosity of the vapor phase are sufficient to achieve such an accuracy. For the existing surface tension data the uncertainty is estimated to be better than ±1.2%. A more detailed discussion regarding the accuracy achievable for liquid kinematic viscosity and surface tension from SLS can be found in Refs. 21 and 23.

For the complete temperature range studied in the present investigation, a modified Andrade-type equation, which in its simple form is commonly chosen to represent the dynamic viscosity at least over a limited temperature range, was used in the form,

$$\nu' = \nu'_0 \exp[\nu'_1 T^{-1} + \nu'_2 T + \nu'_3 T^{-2}] \tag{12}$$

in order to represent our experimental kinematic viscosity data for R365mfc, where T is the temperature in K and the coefficients are given in Table VI. Here, also the standard deviation of our data relative to those calculated by Eq. (12) is reported. It should be noted that the residuals of the experimental data from the fit are smaller than the standard deviations of the individual measurements which were in all cases smaller than 1.0%.

The experimental data for the surface tension can be well represented by a modified van der Waals-type surface tension equation of the form [29],

$$\sigma = \sigma_0 (1 - T_R)^{1.26} \left[1 + \sigma_1 (1 - T_R)^{0.5} + \sigma_2 (1 - T_R) \right], \tag{13}$$

where the fit parameters σ_0, σ_1, and σ_2 are given in Table VII. In Eq. (13) $T_R = T/T_C$ represents the reduced temperature, where T is the abso-

Table VII. Coefficients of Eq. (13)

σ_0 (mN·m^{-1})	71.176
σ_1	–0.5836
σ_2	0.3881
rms (%)	0.39
T-range (K)	253–373

lute temperature and T_C is the critical temperature. For the latter, a value of (460 ± 1) K was estimated by extrapolating the correlation, Eq. (11), for the values of the thermal diffusivity which vanish if the critical point is reached. The present correlation, Eq. (13), represents the experimental values of the surface tension with a root-mean-square deviation of about 0.4%.

4. CONCLUSIONS

In the present study several thermophysical properties of the new fluoroalkane R365mfc have been determined, which serves as one principal component in blends of technical interest, e.g., in the field of high-temperature heat-pump systems. For the liquid phase, the density and thermal conductivity have been obtained by conventional measurement techniques at or near saturation conditions, respectively. The thermal diffusivity, sound speed, liquid kinematic viscosity, and surface tension have been measured under true saturation conditions over a wide temperature range using light scattering techniques. Due to the lack of reference data, only the experimental values for the liquid density could be discussed in comparisons to literature. For all other properties—to the best of our knowledge—the present study provides the first data for R365mfc.

ACKNOWLEDGMENTS

The investigated refrigerant sample has been provided by Solvay Fluor and Derivate GmbH, Hannover. We thank Lara Penedo Pellegrino for her valuable assistance in carrying out many of the experiments.

REFERENCES

1. Solvay Fluor and Derivate GmbH, *Solkane*® 365/227 *Non Flammable Blends—Liquid Foaming Agent for Plastics*, Hannover (2002).
2. H. Krähling and L. Zipfel, *Proc. Polyurethanes Conference* (Boston, 2000), pp. 23–31.

3. R. Heidelck, H. Kruse, and H.-J. Laue, *Wärmepumpen in Gewerbe und Industrie—Ein Überblick*, Informationszentrum Wärmepumpen und Kältetechnik e.V., Hannover (2000).
4. D. S. Jung and D. Didion, *Int. J. Refrig.* **13**: 243 (1990).
5. R. Heide and J. Schenk, in *Bestimmung der Transportgrößen* von HFKW, Bericht zum AiF-Forschungsvorhaben Nr. 10044B, Heft 1: Viskosität und Oberflächen spannung, Forschungsrat Kälte technik e.V., ed. (Frankfurtam Main, 1996).
6. N. Hoffmann, K. Spindler, and E. Hahne, in *Bestimmung der Transportgrößen von HFKW*, Bericht zum AiF-Forschungsvorhaben Nr. 10044B, Heft 2: Wärme leitfähigkeit, Forschungsrat Kältetechnik e.V., ed. (Frankfurt am Main, 1996).
7. X. Gao, M. J. Assael, Y. Nagasaka, and A. Nagashima, *Int. J. Thermophys.* **21**: 23 (2000).
8. A. P. Fröba, S. Will, and A. Leipertz, *Int. J. Thermophys.* **22**: 1349 (2001).
9. I. M. Marrucho, N. S. Oliveira, and R. Dohrn, *J. Chem. Eng. Data* **47**: 554 (2002).
10. K. Börner, *private communication,* Technical Service Foam, Solvay Fluor and Derivate GmbH, Hannover (2003).
11. M. L. V. Ramires, C. A. Nieto de Castro, Y. Nagasaka, A. Nagashima, M. J. Assael, and W. A. Wakeham, *J. Phys. Chem. Ref. Data* **24**: 1377 (1995).
12. N. B. Vargaftik, *Tables on the Thermophysical Properties of Liquids and Gases in Normal and Dissociated States* (Hemisphere, Washington, D.C., 1983).
13. K. Krzeminski, A. P. Fröba, and A. Leipertz, submitted for publication to Chemie Ingenieur Technik (2003).
14. B. J. Berne and R. Pecora, *Dynamic Light Scattering* (Robert E. Krieger, Malabar, 1990).
15. B. Chu, *Laser Light Scattering* (Academic Press, New York, 1991).
16. J. N. Shaumeyer, R. W. Gammon, and J. V. Sengers, in *Measurement of the Transport Properties of Fluids*, W. A. Wakeham, A. Nagashima, and J. V. Sengers, eds. (Blackwell Scientific, Oxford, 1991), pp. 197–213.
17. A. Leipertz and A. P. Fröba, in *Diffusion in Condensed Matter—Methods, Materials, Models*, P. Heitjans and J. Kärger, eds. (Springer, Berlin, 2004), pp. 571–611.
18. S. Will, A. P. Fröba, and A. Leipertz, *Int. J. Thermophys.* **19**: 403 (1998).
19. A. P. Fröba, S. Will, and A. Leipertz, *Fluid Phase Equilib.* **161**: 337 (1999).
20. D. Langevin, *Light Scattering by Liquid Surfaces and Complementary Techniques* (Marcel Dekker, New York, 1992).
21. A. P. Fröba, *Simultane Bestimmung von Viskosität und Oberflächenspannung transparenter Fluide mittels Oberflächenlichtstreuung*, Dr.-Ing. Thesis, Friedrich-Alexander-Universität Erlangen-Nürnberg, Erlangen (2002).
22. E. H. Lucassen-Reynders and J. Lucassen, *Advan. Colloid Interface Sci.* **2**: 347 (1969).
23. A. P. Fröba and A. Leipertz, *Int. J. Thermophys.* **24**: 895 (2003).
24. www.solvay-fluor.com/docroot/fluor/static_files/attachments/druck_365_e.pdf
25. C. Meurer, *private communication*, Technical Services Refrigerants, Solvay Fluor and Derivate GmbH, Hannover (2003).
26. K. Kraft, M. M. Lopes, and A. Leipertz, *Int. J. Thermophys.* **16**: 423 (1995).
27. K. Lucas, *C. I. T.* **46**:157 (1974).
28. R. C. Reid, J. M. Prausnitz, and B. E. Poling, *The Properties of Gases and Liquids* (McGraw-Hill, New York, 1977 and 1987).
29. C. Miqueu, D. Broseta, J. Satherley, B. Mendiboure, J. Lachaise, and A. Graciaa, *Fluid Phase Equilib.* **172**: 169 (2000).